Hofstadter butterflies in macroscopic time-reversal invariant systems: Tight-binding electrons under $n\sqrt{2}\times n\sqrt{2}$ staggered magnetic fields

Yi-Fei Wang[1] and Chang-De Gong[2,1]
[1]*Research Center for Quantum Correlation, Department of Physics, Nanjing University, Nanjing 210093, China*
[2]*Chinese Center of Advanced Science and Technology (World Laboratory), P. O. Box 8730, Beijing 100080, China*
(Received 25 April 2006; revised manuscript received 23 September 2006; published 3 November 2006)

Hofstadter's diagrams (the energy spectra plotted against the magnetic flux strength ϕ) of tight-binding lattice electrons under $n\sqrt{2}\times n\sqrt{2}$ staggered magnetic fields are obtained for various n's. From $n=1-14$, these butterflylike continuous spectrum diagrams exhibit a systematic evolution approaching the fractal Hofstadter butterfly spectrum. For larger n's, these butterflies can be roughly divided into two kinds of regions, the "Hofstadter-type regions" which bear the fractal structures, and the "non-Hofstadter-type regions" which are composed of almost equally spaced subbands. The properties of electronic states in the non-Hofstadter-type regions are revealed in detail.

DOI: 10.1103/PhysRevB.74.193301 PACS number(s): 73.21.−b, 75.10.Lp, 71.20.−b, 71.70.Di

Over the past two decades, the orbital dynamics of two-dimensional (2D) electrons coupled to a uniform perpendicular magnetic field has been of special interest in condensed matter physics. Even when electrons may be considered as noninteracting, remarkable features of the one-particle spectrum, illustrated by the well-known Hofstadter butterflylike diagram,[1–3] take place in the presence of a square lattice due to the subtle commensurability between two area scales in this system: one is imposed by the lattice periodicity and the other is imposed by the uniform magnetic field.

For an experimental realization of the butterfly with typical lattice spacings of only a few angstroms, magnetic fields of about 10^4 T are necessary, which is far beyond the technically accessible limit. There exist several ways to circumvent this problem by utilizing artificial systems, e.g., lateral superlattices produced with high-quality shallow heterostructures,[4] Wigner crystals formed by the crystallization of an electron gas,[5] microwave waveguides based on an analogy between electronic and photonic systems,[6] superconducting wire networks,[7] and optical lattices with confined cold atoms.[8]

There are two lines to further theoretical investigations of Hofstadter's problem. One line is to consider different 2D structures, such as triangular,[9] honeycomb,[10] and kagomé lattices,[11] lateral superlattices,[12] superstructures with flat bands,[13] quasiperiodic tilings,[14] fractal networks,[15,16] and rhombus tilings.[17]

Another line is to consider different magnetic fields, such as fields that are spatially sine or cosine modulated,[18–20] staggered-modulated,[21,22] and strip modulated.[22] The field modulation generically breaks the symmetries and the fractal property of the Hofstadter spectrum.[20] There is an interesting but inconsistent result in the relevant works. Gumbs and co-workers[18] argued that the field modulation leads to an additional crisscross pattern like a spider-web structure on the Hofstadter butterfly. However, the results by Oh[20] indicate that there is no additional spider-web structure in the energy spectrum.

To the best of our knowledge, all the systems of previous studies are time-reversal (and space-inversion) symmetry broken both microscopically and macroscopically. We would address the following problems: Can the Hofstadter butterfly be produced in a macroscopic time-reversal invariant system? If so, how does it differ from the conventional one? What is special about the properties of the electronic states?

To answer the above problems, we study tight-binding electron systems embedded in a square lattice under a series of $n\sqrt{2}\times n\sqrt{2}$ staggered magnetic fields with various n's. In contrast to all the above systems, our system is macroscopically space-inversion and time-reversal invariant since the total magnetic flux through any square area with the size $n\sqrt{2}a\times n\sqrt{2}a$ (a is the lattice constant) is zero. Recently, adopting a superconductor-ferromagnet hybrid system consisting of a superconducting wire network and an array of mesoscopic ferromagnets, magnetic fields with similar configurations have been realized experimentally.[22,23] Therefore our investigation is not only based on theoretical interest, and our results should be experimentally realizable with such artificial systems.

The following U(1) gauge-invariant tight-binding Hamiltonian describes the orbital dynamics of the electrons under an $n\sqrt{2}\times n\sqrt{2}$ staggered magnetic field:

$$H=-t\sum_{\langle ij\rangle\sigma}(e^{i\phi_{ij}}c_{j\sigma}^{\dagger}c_{i\sigma}+\text{H.c.}). \tag{1}$$

Here ϕ_{ij} is in units of $\phi_0/2\pi$ ($\phi_0=hc/e$ is the flux quantum). The nearest-neighbor hopping integral of electrons t is modified as $t_{ij}=t\exp(i\phi_{ij})$ because electron hopping from one site to its nearest neighbors should suffer a phase shift due to the Aharonov-Bohm effect. Selection of these phase shifts ϕ_{ij} is shown in Fig. 1 for $n=3$ and it ensures that electrons circling a plaquette once suffer a total phase shift $\pm\phi$ (the Hofstadter diagram and other physical properties are gauge invariant).

A magnetic unit cell should have integer flux quanta. In our problem, the total magnetic flux through any square area with the size $n\sqrt{2}a\times n\sqrt{2}a$ is zero, namely, the corresponding magnetic unit cell has the size $n\sqrt{2}a\times n\sqrt{2}a$. Therefore the introduction of a $n\sqrt{2}\times n\sqrt{2}$ staggered magnetic field splits the original ($\phi=0$) tight-binding band into $2n^2$ subbands [each one contributes $1/(2n^2)$ fraction to the total density of states (DOS)]. This is in contrast to the conventional case of a uniform magnetic field where the magnetic unit cells and the number of subbands depend on the values of the mag-

 ©2006 The American Physical Society

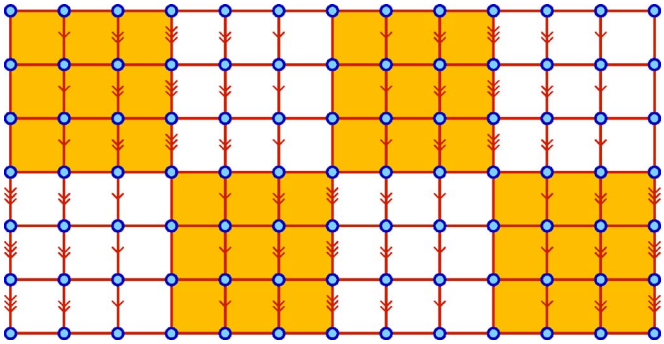

FIG. 1. (Color online) Illustration of the square lattice under an $n\sqrt{2}\times n\sqrt{2}$ staggered magnetic field with $n=3$ and the selected gauge. A plaquette filled with color has a flux ϕ, and a blank one has a flux $-\phi$. Each arrow represents a phase shift ϕ in its direction.

netic flux ϕ. After the Fourier transformation, the Hamiltonian of our problem can be written as a $2n^2\times 2n^2$ matrix in k space. Then the $2n^2$ branches of energy spectra are obtained through the numerical diagonalization of the Hamiltonian matrix in k space.

Hofstadter diagrams for different n's from 1 to 14 have been calculated, as illustrated in Fig. 2. In contrast to the conventional way of plotting Hofstadter diagrams in literature, we use gray scale contour plots. Therefore not only the regions where there are energy spectra have been shown, but also the magnitudes of the density of states are displayed with various gray scales. There are many discernible lines in the diagrams shown in Fig. 2. These lines exhibit the evolutions of the logarithmic van Hove singularities (one singularity per subband) and the finite discontinuities (or the subband edges) in the DOS versus the magnetic flux ϕ. All these lines are periodic and continuous functions of ϕ with the period 2π.

For $n=1$, 2 [Figs. 2(a) and 2(b)], the diagrams do not show any resemblance to the conventional Hofstadter butterfly. For $n=3$, 4, and 5 [Figs. 2(c)–2(e)], the diagrams look butterflylike. The lowest and the highest subbands accumulate separately near $\phi=\pi$ (half-flux quantum per plaquette), and form the backbones of two butterflies. For $n=7$, 10, and 14 [Figs. 2(f)–2(h)], the diagrams can be divided into two kinds of regions. One kind of region is the allowed band region in the conventional Hofstadter butterfly, and bears some fractal structures. We thus name them "Hofstadter-type regions." Another kind of region is the gap region in the conventional Hofstadter butterfly, and is composed of almost equally spaced subbands. We thus name them "non-Hofstadter-type regions." For $n=14$, the diagram looks quite similar to the conventional Hofstadter butterfly.

To get a closer look at the non-Hofstadter-type regions, the DOS for the spectra at $\phi=0.5\pi$ are plotted in Fig. 3 for $n=7$, 10, and 14. Given n, there are several tadpolelike Landau subbands in the DOS, which are similar in shape and size and almost equally spaced. When n increases from 7 to 10 and then 14, these DOSs change as follows: the number of subbands in the non-Hofstadter-type regions is increased; the spectral weight in the non-Hofstadter-type regions η_{non} $(=1-\eta_{\text{Hof}})$ are transferred to the Hofstadter-type regions. We can estimate the spectra weight in the non-Hofstadter-type

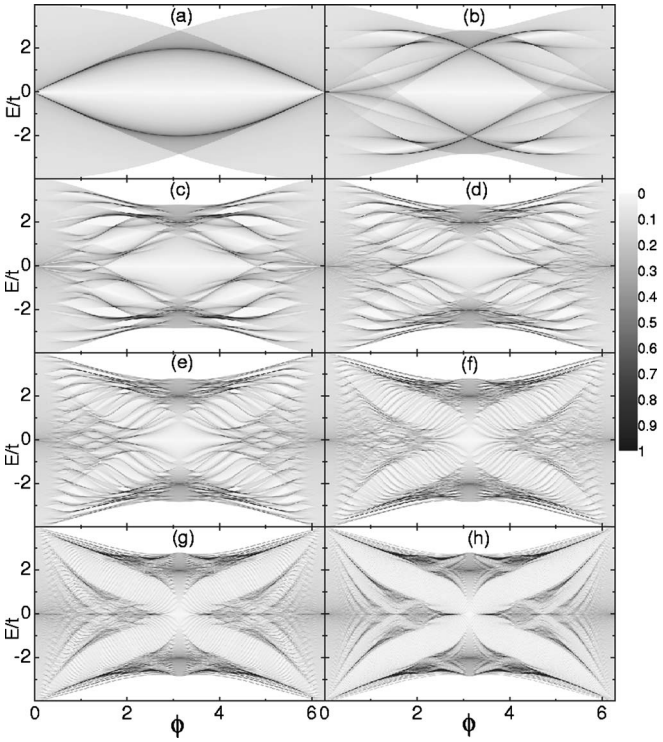

FIG. 2. Gray-scale contour plots for Hofstadter's diagrams (the energy spectra against the magnetic flux strength ϕ) of $n\sqrt{2}\times n\sqrt{2}$ staggered magnetic fields. The various gray scales represent the magnitudes of the DOS of the energy spectra: (a) $n=1$, (b) $n=2$, (c) $n=3$, (d) $n=4$, (e) $n=5$, (f) $n=7$, (g) $n=10$, and (h) $n=14$.

regions roughly by counting the number of subbands therein: $\eta_{\text{non}}^{n=7}=\frac{3}{49}>\eta_{\text{non}}^{n=10}=\frac{5}{100}>\eta_{\text{non}}^{n=14}=\frac{7}{196}$.

The appearance of the non-Hofstadter-type regions is quite similar to the spider-web structure appearing in the paper by Gumbs *et al.*[18] Later prudent and detailed studies by Oh[20] showed that the spider-web structure was erroneous, arising from mistakes in choosing the values of modulation parameters and k vectors. Therefore, the non-Hofstadter-type regions in our cases could be the convincing superimposed structures in addition to the Hofstadter fractal ones.

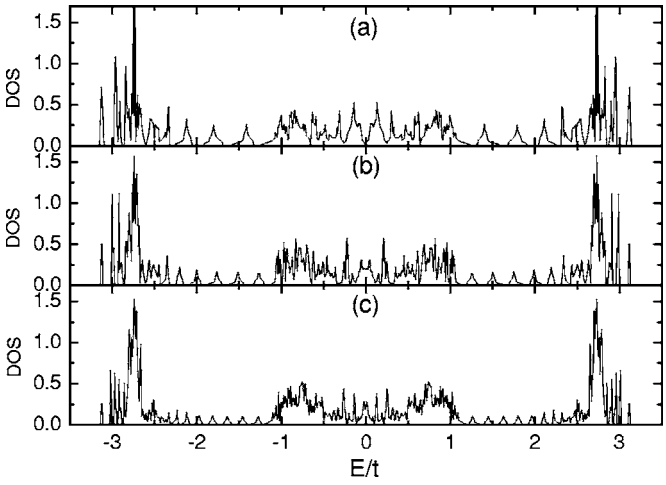

FIG. 3. DOS for $\phi=0.5\pi$. $n=$ (a) 7; (b) 10; (c) 14.

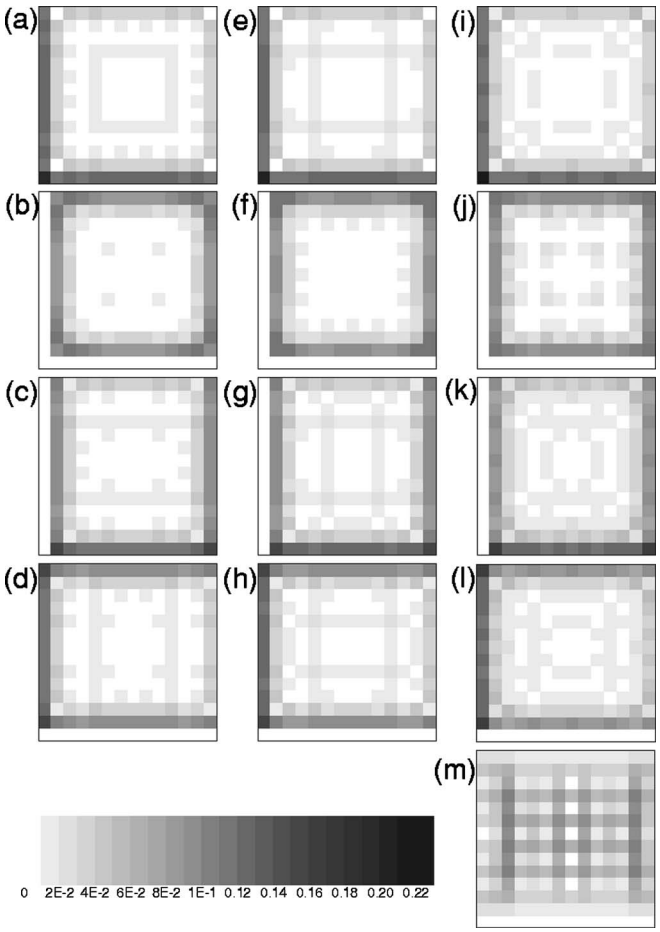

FIG. 4. Spatial variation of $|\psi_i|$ at 14×14 sites for $n=14$, $\phi=\pi/2$, and $(k_x,k_y)=(0,0)$. The cases (a)–(l) correspond to 12 sequential electronic states (from the 93rd state with the energy $E^{(93)}=-2.32t$ to the 104th state with $E^{(104)}=-1.41t$) in the non-Hofstadter-type regions, while the case (m) corresponds to an electronic state (the 20th state with $E^{(20)}=-2.81t$) in the Hofstadter-type regions.

For n larger than 14, we argue that the spectra will exhibit fractal properties in more and more details, and the non-Hofstadter-type regions will disappear in the large-n limit; namely, in this limit, an $n\sqrt{2}\times n\sqrt{2}$ staggered magnetic field is equivalent to a uniform one in the energy-spectral aspect. The arguments are quite reasonable: the $n\sqrt{2}\times n\sqrt{2}$ staggered magnetic field divides the 2D space into two kinds of plaquettes, which have the size $n\times n$; electrons moving in the central regions of the plaquettes (which contribute to the Hofstadter-type regions in the spectra) do not "feel" the presence of boundaries between these plaquettes (when only nearest-neighbor hopping is considered); when n is increased, the ratio of electrons moving in the boundary regions (which contribute to the non-Hofstadter-type regions in the spectra) versus the total electrons will decrease substantially.

Now we investigate the properties of the electronic states in the non-Hofstadter-type regions. In the following, we concentrate on the case $n=14$, $\phi=\pi/2$ and study the electronic states with a fixed wave vector $(k_x,k_y)=(0,0)$ and various energies. The ith site component of a real-space wave function Ψ is denoted as ψ_i. In Figs. 4(a)–4(l), we plot the spatial variation of $|\psi_i|$ for 12 sequential electronic states (from the 93rd state $\Psi^{(93)}$ with the energy $E^{(93)}=-2.32t$ to the 104th state $\Psi^{(104)}$ with $E^{(104)}=-1.41t$) at 14×14 sites (which is verified as the spatial period of $|\psi_i|$).

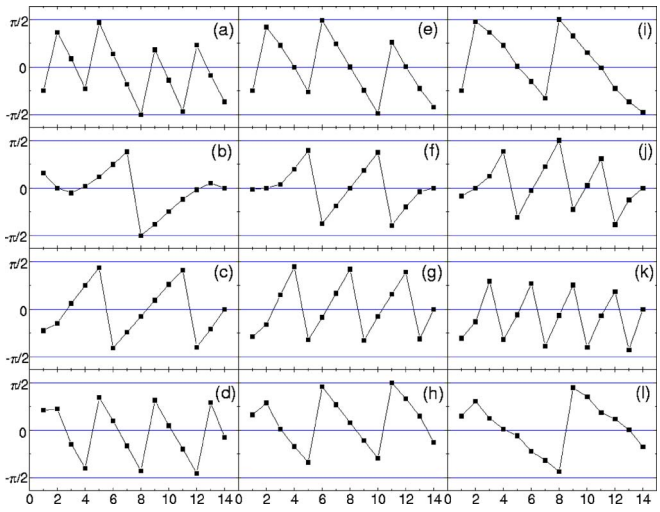

FIG. 5. (Color online) Spatial variation of arg ψ_i along the left edge of each boundary state in Figs. 4(a)–4(l).

We can see that these 12 states are generically localized at either square or rectangular edges. [In contrast, a state in the Hofstadter-type regions, e.g., the 20th state in Fig. 4(m) with $E^{(20)}=-2.81t$, is extended over almost the whole region.] We divide these 12 states into three groups and each group has a 15×15 boundary state, a 13×13 one, a 13×15 one, and a 15×13 one in sequence: $\{\Psi^{(93)},\Psi^{(94)},\Psi^{(95)},\Psi^{(96)}\}$, $\{\Psi^{(97)},\Psi^{(98)},\Psi^{(99)},\Psi^{(100)}\}$, $\{\Psi^{(101)},\Psi^{(102)},\Psi^{(103)},\Psi^{(104)}\}$. We note that in each group two square boundary states have very close energies (e.g., $E^{(97)}=-2.02t$ and $E^{(98)}=-1.99t$), and two rectangular boundary states have the same energies: (e.g., $E^{(99)}=E^{(100)}=-1.76t$).

In order to inquire into the problem of what kind of quantization is responsible for the equal energy spacing in the non-Hofstadter-type regions, we plot in Fig. 5 the spatial variation of the argument of ψ_i, i.e., arg ψ_i $=\arctan(\mathrm{Im}\,\psi_i/\mathrm{Re}\,\psi_i)$, along the left edge for each of the above 12 boundary states. We can see that, for each kind of boundary state in the three groups, arg ψ_i exhibits periodic fluctuation. We focus on the first row of Fig. 5 which corresponds to the first state of each group (the 15×15 boundary state) with almost equal energy spacing ($E^{(93)}=-2.32t$, $E^{(97)}=-2.02t$, and $E^{(101)}=-1.69t$). It is clear that the periods of arg ψ_i for the three 15×15 boundary states are 4, 3, and 2 and hence exhibit quantized behavior. And for the other three kinds of boundary states, arg ψ_i also show similar quantized behavior.

In summary, we have obtained Hofstadter diagrams of a macroscopical space-inversion and time-reversal invariant system, i.e., a system of tight-binding lattice electrons under $n\sqrt{2}\times n\sqrt{2}$ staggered magnetic fields. From $n=1$ to 14, these butterflylike continuous spectrum diagrams exhibit a systematic evolution approaching the fractal Hofstadter butterfly spectrum. For larger n's, these butterflies can be divided into

two kinds of regions: Hofstadter-type regions which bear the fractal structures, and non-Hofstadter-type regions which appear in gap regions of the conventional Hofstadter butterfly and are composed of almost equally spaced subbands. When n is increased, the spectra weight of the non-Hofstadter-type regions is reduced and transferred to the Hofstadter-type regions gradually. The electronic states in the non-Hofstadter-type regions are generically localized at either square or rectangular edges, and the arguments of wave-function components at boundary sites exhibit quantized behavior which is responsible for the equal energy spacing.

This work is supported by the Chinese National Natural Science Foundation.

[1] D. R. Hofstadter, Phys. Rev. B **14**, 2239 (1976).
[2] G. H. Wannier, Phys. Status Solidi B **88**, 757 (1978).
[3] G. H. Wannier, G. M. Obermair, and R. Ray, Phys. Status Solidi B **93**, 337 (1979).
[4] T. Schlösser *et al.*, Europhys. Lett. **33**, 683 (1996); C. Albrecht *et al.*, Phys. Rev. Lett. **86**, 147 (2001); M. C. Geisler *et al.*, *ibid.* **92**, 256801 (2004).
[5] I. N. Harris *et al.*, Europhys. Lett. **29**, 333 (1995).
[6] U. Kuhl and H. J. Stöckmann, Phys. Rev. Lett. **80**, 3232 (1998).
[7] B. Pannetier *et al.*, J. Phys. (Paris), Lett. **44**, L853 (1983); B. Pannetier, J. Chaussy, R. Rammal, and J. C. Villegier, Phys. Rev. Lett. **53**, 1845 (1984); B. Pannetier *et al.*, Surf. Sci. **229**, 331 (1990); C. C. Abilio *et al.*, Phys. Rev. Lett. **83**, 5102 (1999).
[8] D. Jaksch and P. Zoller, New J. Phys. **5**, 56 (2003); E. J. Mueller, Phys. Rev. A **70**, 041603(R) (2004); A. S. Sørensen, E. Demler, and M. D. Lukin, Phys. Rev. Lett. **94**, 086803 (2005); K. Osterloh, M. Baig, L. Santos, P. Zoller, and M. Lewenstein, *ibid.* **95**, 010403 (2005).
[9] F. H. Claro and G. H. Wannier, Phys. Rev. B **19**, 6068 (1979).
[10] R. Rammal, J. Phys. (Paris) **46**, 1345 (1985).
[11] Y. Xiao, V. Pelletier, P. M. Chaikin, and D. A. Huse, Phys. Rev. B **67**, 104505 (2003).
[12] M. A. Andrade Neto and P. A. Schulz, Phys. Rev. B **52**, 14093 (1995).
[13] H. Aoki, M. Ando, and H. Matsumura, Phys. Rev. B **54**, R17296 (1996).
[14] A. Behrooz *et al.*, Phys. Rev. Lett. **57**, 368 (1986); K. Springer and D. van Harlingen, Phys. Rev. B **36**, 7273 (1987); H. Schwabe, G. Kasner, and H. Böttger, *ibid.* **56**, 8026 (1997).
[15] B. Douçot *et al.*, Phys. Rev. Lett. **57**, 1235 (1986); J. M. Gordon *et al.*, *ibid.* **56**, 2280 (1986).
[16] Q. Niu and F. Nori, Phys. Rev. B **39**, 2134 (1989).
[17] J. Vidal, R. Mosseri, and B. Douçot, Phys. Rev. Lett. **81**, 5888 (1998).
[18] G. Gumbs, D. Miessein, and D. Huang, Phys. Rev. B **52**, 14755 (1995).
[19] G. Y. Oh and M. H. Lee, Phys. Rev. B **53**, 1225 (1996).
[20] G. Y. Oh, Phys. Rev. B **60**, 1939 (1999).
[21] Q. W. Shi and K. Y. Szeto, Phys. Rev. B **56**, 9251 (1997).
[22] Y. Iye, E. Kuramochi, M. Hara, A. Endo, and S. Katsumoto, Phys. Rev. B **70**, 144524 (2004).
[23] S. Ito, M. Ando, S. Katsumoto, and Y. Iye, J. Phys. Soc. Jpn. **68**, 3158 (1999); M. Ando, S. Ito, S. Katsumoto, and Y. Iye, *ibid.* **68**, 3462 (1999).